Title
Acoustic-based measurements of material absorption coefficients: Relationship between laser pulse duration and stress confinement time

Journal
Journal of Applied Physics, 94(12)

ISSN
0021-8979

Authors
Choi, Bernard
Jansen, E Duco
Welch, Ashley J

Publication Date
2003-12-15

DOI
10.1063/1.1627464

Acoustic-based measurements of material absorption coefficients: Relationship between laser pulse duration and stress confinement time

Bernard Choi[a)]
Department of Biomedical Engineering, The University of Texas at Austin, Austin, Texas 78712 and Beckman Laser Institute, University of California, Irvine, California 92612

E. Duco Jansen
Department of Biomedical Engineering, Vanderbilt University, Nashville, Texas 37235

Ashley J. Welch
Department of Biomedical Engineering, The University of Texas at Austin, Austin, Texas 78712

(Received 21 July 2003; accepted 24 September 2003)

Ideally, to use photoacoustics to determine the absorption coefficient μ_a of a medium, the laser pulse duration τ_p is much shorter than the stress confinement time τ_{sr} required for a laser-induced stress wave to propagate a distance equal to the light penetration depth δ. However, without prior knowledge of δ (equal to $1/\mu_a$), it is not clear whether a given photoacoustic measurement is indeed performed under stress-confined conditions. The purpose of this study was to explore the effects of τ_p and τ_{sr} upon efforts to obtain estimates of μ_a using photoacoustics. A numerical model was developed to simulate stress signals and investigate how measurements of μ_a are related to the ratio $\tau = \tau_p/\tau_{sr}$. Experimental photoacoustic measurements at several values of τ were performed to estimate μ_a of water, and a deconvolution model was applied to correct the measured μ_a without prior knowledge of τ. Under the conditions simulated in this study, τ_p must be less than $\sim 0.1\tau_{sr}$ for optimal photoacoustic measurements of μ_a. Since it is difficult to achieve such conditions at midinfrared wavelengths for accurate soft tissue characterization due to strong water absorption bands, a numerical deconvolution technique was implemented to overcome this limitation of conventional photoacoustics, resulting in up to a 30% improvement in photoacoustic-based estimates of the sample μ_a. [DOI: 10.1063/1.1627464]

I. INTRODUCTION

Accurate knowledge of tissue optical properties is critical for development of light-based diagnostic and therapeutic technologies. Both direct and indirect techniques are employed to determine these parameters. With indirect techniques such as spectrophotometry[1,2] and pulsed photothermal radiometry,[3,4] complex algorithms are required to determine absorption and scattering properties from the measured signals. Photoacoustics provides a direct means to measure tissue properties using a wide band acoustic transducer to detect stress waves induced by short laser pulses.[5] Ideally, the laser pulse duration τ_p is much shorter than the stress confinement time τ_{sr} required for a laser-induced stress wave to propagate a distance equal to the light penetration depth δ. τ_{sr} is defined as

$$\tau_{sr} = \delta / c_s, \tag{1}$$

where c_s is the speed of sound in the medium (1.5×10^5 cm/s in water, which is similar to the value for biological soft tissue). Under stress confinement conditions (e.g., $\tau_p \ll \tau_{sr}$), the measured stress signal shape represents exactly the light distribution in the medium. Absorption and scattering coefficients (μ_a and μ_s, respectively) are determined from these profiles. For homogeneous media, these parameters are identified from examination of the peak value and exponential decay of the profiles. Viator *et al.*[6] derived a relatively simple technique for using photoacoustics to determine μ_a values of layered tissue phantoms.

At visible and near-infrared wavelengths ($\lambda = 0.4$–$1.1\ \mu$m), *Q*-switched lasers emitting pulses of $\tau_p = 1$–10 ns are readily available. At midinfrared wavelengths ($\lambda = 2$–$10\ \mu$m), conventional *Q*-switched solid-state lasers provide longer pulses of $\tau_p \geq 100$ ns. Without prior knowledge of δ (equal to $1/\mu_a$), it is not clear whether a given photoacoustic measurement is indeed performed under stress-confined conditions. For experiments at midinfrared laser wavelengths on tissue with high water and/or protein content, μ_a values range over several orders of magnitude, from ~ 10 to over 10 000 cm^{-1}, corresponding to τ_{sr} between 0.1 and 1000 ns. Under these conditions, the relationship between τ_p and τ_{sr} is of paramount importance. The purpose of this study is to explore the effects of τ_p and τ_{sr} on μ_a values ascertained with photoacoustics. A numerical model was developed to simulate stress signals and investigate how measurements of μ_a is related to the ratio $\tau = \tau_p/\tau_{sr}$. Experimental photoacoustic measurements at several values of τ were performed to estimate μ_a of an absorbing medium (water), and a deconvolution model was applied

[a)]Author to whom correspondence should be addressed; present address: Beckman Laser Institute, University of California, Irvine, 1002 Health Sciences Road East, Irvine, CA 92612; electronic mail: bchoi@laser.bli.uci.edu

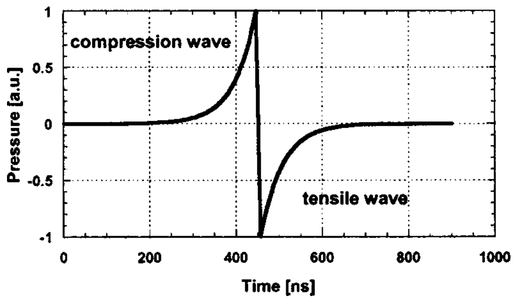

FIG. 1. Theoretical example of a bipolar stress wave generated under ideal conditions in a homogeneous medium. The first half of the signal is a compression wave and the second half a tensile wave. For the case in which scattering is negligible, the exponential decay constant of either the compression or tensile wave is the absorption coefficient of the medium.

to correct the measurements of μ_a without prior knowledge of τ.

II. MATERIALS AND METHODS

A. Thermoelastic stress wave generation

An ideal acoustic signal induced by a stress-confined laser pulse in a homogeneous medium is shown in Fig. 1. In this example, four conditions are required: (1) light absorption dominates over light scattering; (2) the acoustic transducer is at the backside of the medium and the laser pulse is incident on the front side; (3) acoustic impedance of the medium is greater than that of the surroundings; and (4) δ is at least an order of magnitude less than the spot size, providing a basis for a one-dimensional geometry assumption. Upon pressure generation, half of the pressure signal propagates towards the transducer and the other half towards the medium surface. The first half of the signal is a compression wave. The shape of the compression wave resembles the absorbed energy density distribution inside the medium; the peak at 450 ns (Fig. 1) corresponds to the medium surface and the initial portion of the rise represents deeper regions of the medium. A subsequent tensile wave occurs due to reflection of the acoustic signal from the front surface. Since the compression and tensile waves are exact replicas of the absorbed energy density distribution, μ_a can be calculated either from the peak pressure amplitude or from a Beer's law exponential fit to the data because

$$P(z)=\frac{\Gamma\mu_a H_0\exp(-\mu_a z)}{k'}, \tag{2}$$

where $P(z)$ is the pressure (atm) at depth z, Γ is the Gruneisen coefficient $(-)$, H_0 is the radiant exposure (J/cm^2), and $k'=101\,325$ Pa/atm is a unit conversion factor. Γ represents a measure of heat-to-acoustic energy conversion and is defined as

$$\Gamma=\frac{\beta c_s^2}{c_p}, \tag{3}$$

where β is the thermal coefficient of volume expansion (K^{-1}) and c_p is the specific heat at constant pressure (J/g/K). Each of these parameters is temperature dependent; for water, Γ can be estimated from the following empirically-derived equation:[5]

$$\Gamma=0.0043+0.0053T, \tag{4}$$

where T is temperature (°C).

If $\tau_p>\tau_{sr}$, sufficient time exists for the generated stress wave to propagate beyond δ. Under this condition, μ_a calculations from measured stress signals may underestimate the actual values. As τ_p increases, the degree of underestimation increases and the stress signal shape resembles more closely the laser pulse temporal profile.[5] For $\tau_p\approx\tau_{sr}$, the degree of error associated with photoacoustic-based absorption coefficient measurements is largely unknown.

B. Relationship between τ_p and τ_{sr}—Numerical model

Our model convolves numerically a laser pulse of arbitrary shape with a pressure distribution of arbitrary shape, resulting in a theoretical estimate of the expected stress signal. In this study, the laser pulse temporal profile was assumed to be gaussian shaped, which is typical for many laser systems. The profile was divided arbitrarily into "impulses" with duration $0.01\tau_{sr}$. In this study, the pressure distribution was assumed to follow the shape

$$P(z)=\sum_i \Gamma H_{o,i}\mu_a\exp(-\mu_a z) \tag{5}$$

where $P(z)$ is depth-resolved pressure (bars) induced by the laser pulse and $H_{o,i}$ is input radiant exposure (J/cm^2) of each impulse.

In this study, we assumed the following: (1) medium absorption coefficients $\mu_{a,\text{med}}$ with values ranging between 10 and 1000 cm^{-1}; and (2) τ_p between 1 and 5000 ns. Stress signals were computed and the theoretical estimate of the photoacoustic-based absorption coefficient measurement $\mu_{a,\text{pred}}$ calculated and compared to $\mu_{a,\text{med}}$.

C. Relationship between τ_p and τ_{sr}—Experiments

In this phase of the study, we acquired photoacoustic-based measurements of μ_a for a range of τ and μ_a. Deionized water was used as a homogeneous absorbing medium since values of water μ_a are abundant in the literature and it is the primary constituent of soft tissue. Since water μ_a exhibits a strong wavelength dependence in the midinfrared, different $\mu_{a,\text{med}}$ values were obtained by using different laser wavelengths. Two laser systems were used. A commercial Ho:yttritium–aluminum–garnet (YAG) laser emitted light at 2.1 μm, and was used in Q-switched mode with a measured pulse duration of 819 ± 145 ns. The Vanderbilt free electron laser (FEL) was used as a tunable light source at wavelengths of 2.4 and 3.7 μm.

For the Ho:YAG laser experiment, the optical setup (Fig. 2) consisted of an intracavity acousto-optic modulating Q switch, mirrors to steer the beam, and beam expansion optics to achieve a laser spot diameter of ~3 mm. Portions of the incident beam were sampled with an InAs photodiode (J12-18C-R250U, Judson Technologies, Montgomeryville, PA) and an energy detector (JP25, Molectron Detector, Inc., Port-

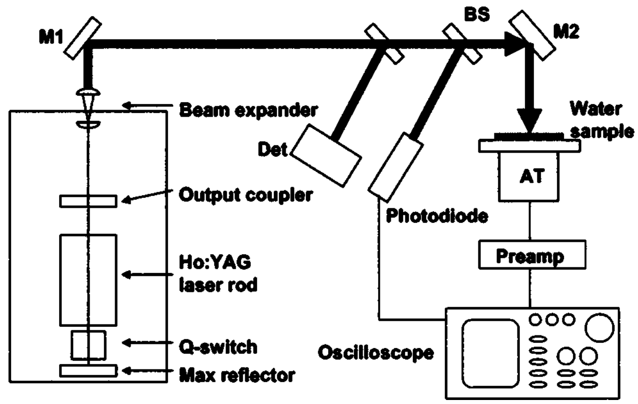

FIG. 2. Optical setup for experiments involving Ho:YAG laser. $M1$, $M2$ = mirrors, BS = beam-splitter, Det = energy detector, AT = acoustic transducer, Preamp = preamplifier.

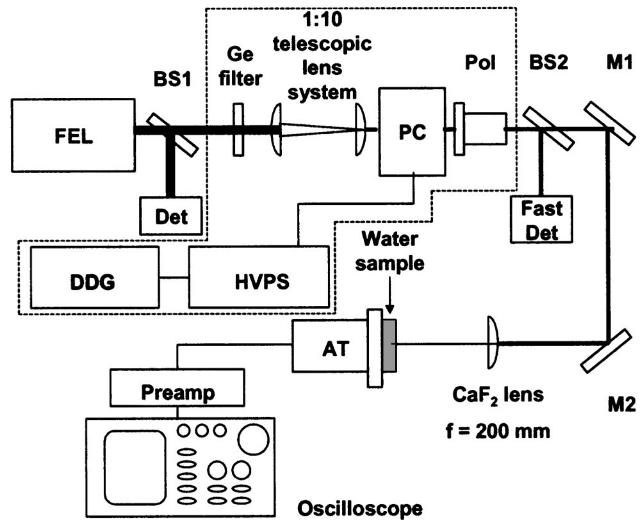

FIG. 3. Optical setups for experiments involving Vanderbilt University FEL. The region enclosed by the dashed lines was used only at $\lambda = 3.7\ \mu$m. BS = beam-splitter, PC = Pockels cell, Pol = polarizer, M = mirror, Det = energy detector, AT = acoustic transducer, Preamp = preamplifier, HVPS = high voltage power supply.

land, OR) to obtain measurements of pulse temporal profile and pulse energy, respectively. The ratio between incident energy and sampled energy was calculated by replacing the acoustic transducer with a second energy detector and simultaneously measuring pulse energies over a wide energy range.

De-ionized water was placed in a 1.4 cm diameter plastic ring located on top of an acoustic transducer (described in the next paragraph). A known volume of water was poured into the ring. Water layer thickness was estimated by dividing the volume by the area of the ring.

The acoustic transducer (WAT-19, LaserSonix, Inc., Houston, TX) consisted of a piezoelectric ceramic element with an aluminum acoustic conductor. It was sensitive to frequencies ranging between 0.5 and 40 MHz. Stress waves reaching the transducer front surface were converted to electrical signals that were subsequently amplified with a low-noise preamplifier (SR445, Stanford Research Systems, Sunnyvale, CA) and acquired with a digital oscilloscope (TDS640A, Tektronix, Beaverton, OR). Laser pulse temporal profiles and acoustic wave forms were stored on the oscilloscope and transferred to PC for postprocessing. To reduce pulse-to-pulse noise, each acquired stress signal was an average of 25 stress waves induced at a pulse repetition rate of 2 Hz, for both lasers.

The FEL is a tunable infrared laser capable of emitting light at wavelengths between 2 and 10 μm. The FEL macropulse consists of 1 ps long micropulses that are spaced 350 ps apart (e.g., 2.85 GHz micropulse repetition rate). A sequence of micropulses results in a macropulse with a duration of approximately 4 μs.

In one set of experiments, the entire FEL macropulse was delivered to the water sample (Fig. 3, excluding region enclosed by the dashed lines). A portion of the beam was sampled with pyroelectric detectors (J8LP and P3-01, Molectron Detector Inc.) to measure pulse energies and temporal profiles, respectively. The beam was focused to the water sample surface using a 200 mm focal length planoconvex CaF_2 lens. The FEL was tuned to a wavelength of 2.4 μm, corresponding to a water μ_a of 50 cm^{-1}.[7]

To investigate the effects of τ_p on photoacoustic-based μ_a measurements, an alternate experimental setup was used (Fig. 3, including region enclosed by a dashed line). The FEL laser wavelength was set at either 2.4 or 3.7 μm (μ_a of water = 50 and 122 cm^{-1}, respectively). A germanium filter was used to remove harmonics of the incident radiation. The beam was then reduced in diameter with a 1:10 telescopic CaF_2 lens system. At 3.7 μm, a CdTe Brewster-cut Pockels cell[8] was used to obtain τ_p ranging between 100 ns and 2 μs. The Pockels cell served as a fast electro-optic shutter; application of a high-voltage ($\sim$3 kV) pulse to the Pockels cell resulted in a transient rotation of the plane of incident linearly polarized light by 90°. A polarizer-attenuator (PAZ-20-AC-4, II-VI, Inc., Saxonburg, PA) placed behind the Pockels cell was set so its plane of polarization was parallel to the 90° rotated light. Light passed through the polarizer attenuator only when the high voltage was applied to the Pockels cell. The duration of the high-voltage pulse was controlled using a digital pulse generator (DG535, Stanford Research Systems).

For both setups, the spot size at the target plane was measured to be $\sim$7 mm diameter, using the knife-edge technique.[9] The transducer and acquisition electronics used in the Ho:YAG experiments described earlier were also used in these experiments.

Software written in LabVIEW (Version 6i, National Instruments, Austin, TX) and MATLAB (Version 6.1, The MathWorks, Natick, MA) was used to process the photoacoustic wave forms. High-frequency noise was removed with a digital second-order Chebyshev low-pass filter [cutoff frequency of $0.01 f_s$, where f_s was the oscilloscope sampling frequency used during signal acquisition (50–500 MHz)]. This filter type was selected to maximize attenuation of frequencies in the stop band and was observed to preserve extremely well the fidelity of the acoustic wave forms. Each time-resolved photoacoustic signal was converted to $P(z)$

profiles by converting time values to depth values using the relationship $z = c_s t$.

First-order exponential decay profiles were fit to the acquired acoustic wave forms using a Levenberg–Marquardt-based nonlinear curve-fit routine.[10] The exponential decay constant was the measured absorption coefficient $\mu_{a,\mathrm{meas}}$. Confidence intervals of 95% of $\mu_{a,\mathrm{meas}}$ were calculated. Box and Whisker plots were used to identify outliers; these data points were not considered in subsequent calculations.

D. Deconvolution model for improved accuracy of absorption coefficient measurements

During the experiments, each laser temporal profile was acquired and saved. A model was developed to predict the stress signal that would result for a given pulse profile and for a range of assumed medium absorption coefficients ($\mu_{a,\mathrm{guess}}$). For a given stress signal measurement, the associated laser pulse temporal profile was reduced to a series of impulses. The duration Δt of each impulse was equal to the shorter of the following values: $1/f_s$, where f_s is the oscilloscope sampling frequency, or $0.01\tau_{sr}$. The factor 0.01 was used because it is reasonable to assume that a pulse with a duration of $0.01\tau_{sr}$ would be considered as stress confined. That is, the pulse would be short enough to create an impulse response. Radiant exposures of each impulse were computed as the energy contained in each impulse divided by the laser spot size.

For each impulse, the resulting bipolar stress wave was modeled as follows. An exponential decay curve calculated with Eq. (2) was generated as a function of time with a decay coefficient equal to $\mu_{a,\mathrm{guess}}$. Γ was assumed to equal 0.121, the value calculated with Eq. (4) at $T = 22\,°\mathrm{C}$. The decay curve was flipped in time to become an exponential growth curve corresponding to the compression stress wave induced by the impulse. Since a free-surface boundary condition and ideal stress generation conditions were assumed, the shape and absolute amplitude of the tensile wave were modeled to be identical to those of the compression wave. Under these assumptions, a bipolar stress wave was created. The stress signal amplitude was scaled according to the fractional energy contained in each impulse.

With each impulse, the corresponding bipolar stress wave was assumed to be generated instantaneously. The onset of subsequent stress signals was separated in time by an integer multiple of Δt. The resulting sequence of impulse responses was summed to form one composite bipolar stress wave.

For direct comparison between measured and modeled stress signals, the modeled signal was "sampled" at frequency f_s and filtered with the same digital low-pass filter used on the measured data. The x axis was converted from units of time to space and an exponential fit applied to the initial rise of the modeled stress signal. The absorption coefficient calculated from the exponential fit represented the prediction of the measured absorption coefficient ($\mu_{a,\mathrm{pred}}$) for a given guess of the sample absorption coefficient $\mu_{a,\mathrm{guess}}$.

For example, consider a scenario in which a 4 μs long pulse with a gaussian temporal profile irradiates a homogeneous sample. $\mu_{a,\mathrm{guess}}$ of 100 cm^{-1} and the pulse temporal profile are inputs into the deconvolution model. A composite stress signal is generated numerically, and an exponential fit to the initial rise of this stress wave results in a calculated absorption coefficient $\mu_{a,\mathrm{pred}}$ of 60 cm^{-1}. The conclusion drawn from this example is that 60 cm^{-1} is the absorption coefficient value that would be measured from an acoustic signal induced in a sample with μ_a of 100 cm^{-1} by a 4 μs long Gaussian-shaped laser pulse.

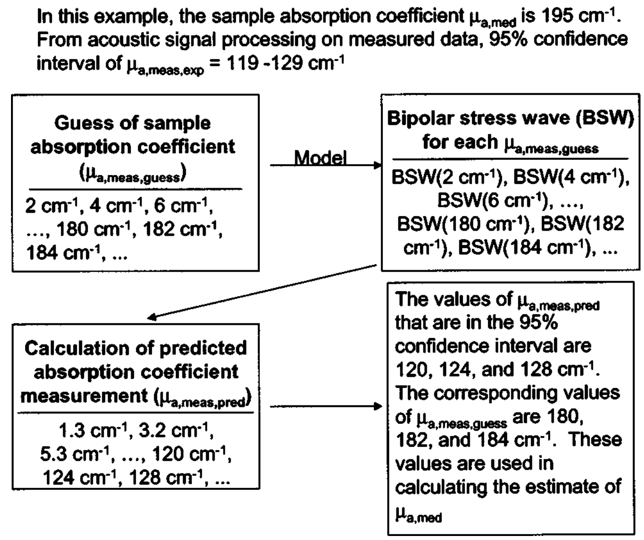

FIG. 4. Example of iterative process used to estimate the actual sample absorption coefficient from measured and model data.

Figure 4 depicts the procedure used to estimate the actual sample absorption coefficient $\mu_{a,\mathrm{med}}$ for any ratio τ. For each measured stress signal, the deconvolution model was run in an iterative fashion. Different $\mu_{a,\mathrm{guess}}$ were input into the model, each resulting in a corresponding bipolar stress wave prediction. The superposition of computed impulse responses resulted in a value of $\mu_{a,\mathrm{pred}}$ based upon $\mu_{a,\mathrm{guess}}$. A set of $\mu_{a,\mathrm{pred}}$ values associated with different $\mu_{a,\mathrm{guess}}$ were compared to the 95% confidence interval range of $\mu_{a,\mathrm{meas}}$ determined from the experimentally measured data. For each value of $\mu_{a,\mathrm{pred}}$ that fell within the 95% range of $\mu_{a,\mathrm{meas}}$, the associated $\mu_{a,\mathrm{guess}}$ was considered as a possible μ_a value. This iterative process was continued until multiple values of $\mu_{a,\mathrm{pred}}$ fell outside of the lower and upper boundaries of the 95% confidence interval. An improved estimate of $\mu_{a,\mathrm{med}}$ was calculated as an average of all possible guesses $\mu_{a,\mathrm{guess}}$.

III. RESULTS

A numerical model was used to investigate the effects of τ_p and τ_{sr} on $\mu_{a,\mathrm{pred}}$ determined from stress signals. For a given τ_p, as $\mu_{a,\mathrm{med}}$ increased, the error in $\mu_{a,\mathrm{pred}}$ increased (Fig. 5). At a specific $\mu_{a,\mathrm{med}}$, the error in $\mu_{a,\mathrm{pred}}$ increased with τ_p. Under the conditions simulated in this study, τ_p must be at most $\sim 0.1\tau_{sr}$ for sufficient stress confinement during the laser pulse so that $\mu_{a,\mathrm{pred}}$ is approximately equal to $\mu_{a,\mathrm{guess}}$.

A representative plot of results obtained with the deconvolution model is shown in Fig. 6. In this example, a 3.7 μm FEL laser pulse temporal profile ($\tau_p = 2\ \mu$s) was input into

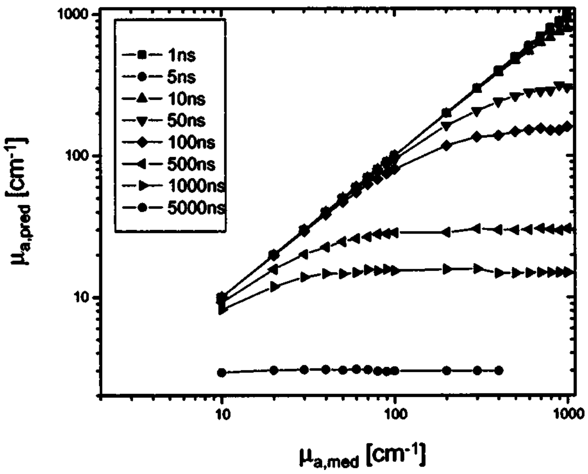

FIG. 5. Log plot of expected photoacoustic-based absorption coefficient measurement ($\mu_{a,\text{pred}}$) vs the actual sample absorption coefficient ($\mu_{a,\text{med}}$) for different laser pulse durations τ_p. Data calculated for $\tau_p = 1$ ns falls on a straight line with slope $= 1$, indicative of sufficient stress confinement for all $\mu_{a,\text{med}}$ values. As τ_p increases, the deviation from this linear relationship increases.

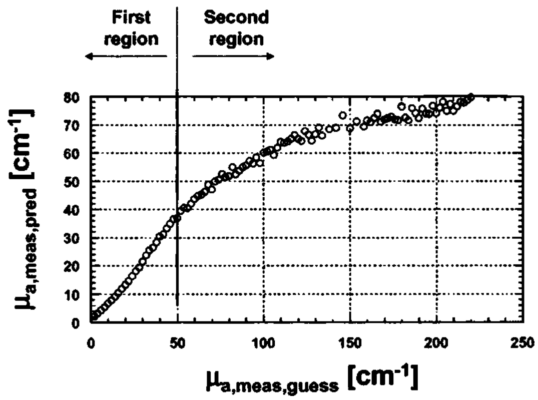

FIG. 6. Representative plot of prediction of absorption coefficient measurement ($\mu_{a,\text{pred}}$) vs the guess of the sample absorption coefficient ($\mu_{a,\text{guess}}$). Two distinct regions of the curve can be identified. In this example, a 3.7 μm FEL laser pulse temporal profile ($\tau_p = 2$ μs) was input into the model.

the model. The range of $\mu_{a,\text{guess}}$ was 2–220 cm^{-1}, and corresponding $\mu_{a,\text{pred}}$ ranged between 2 and 80 cm^{-1}. Note that for larger values of $\mu_{a,\text{guess}}$, the curve appears to approach an asymptotic value for $\mu_{a,\text{pred}}$.

A summary of experimental and deconvolved data is provided in Table I. τ_{sr} at each wavelength was calculated with Eq. (1) using the published values of $\mu_{a,\text{med}}$ for water[7] and c_s of 150 000 cm/s. τ ranged between 1.8 and 37, indicating that all data were taken under conditions of $\tau_p > \tau_{sr}$. For each laser wavelength, μ_a values determined directly from measured data ($\mu_{a,\text{meas}}$) and deconvolved model results ($\mu_{a,\text{pred}}$) are tabulated alongside $\mu_{a,\text{med}}$. The improvement resulting from use of the deconvolution model was determined using the following equation:

$$\%\ \text{improvement} = (|\mu_{a,\text{meas,exp}} - \mu_{a,\text{med}}|/\mu_{a,\text{med}} - |\mu_{a,\text{model}} - \mu_{a,\text{med}}|/\mu_{a,\text{med}}) * 100\%. \tag{6}$$

IV. DISCUSSION

In this study, we investigated the relationship between τ_p, τ_{sr}, and $\mu_{a,\text{meas}}$ for photoacoustic-based measurements of μ_a. A numerical model was employed to determine theoretically the effects of τ_{sr} and τ_p on $\mu_{a,\text{pred}}$. Stress signal measurements were obtained at various τ and $\mu_{a,\text{meas}}$ was extracted from the data. A numerical deconvolution routine was applied to the experimental data to improve the accuracy of the measurements of μ_a. The advantage of using such an approach to determine μ_a is that no prior information about τ is required, which is the case when materials of unknown optical properties at a given laser wavelength are probed, such as kidney stones[11] and thermally denatured skin.[12,13]

Assuming a Gaussian-shaped laser pulse temporal profile and ideal stress signal generation and detection, photoacoustic-based measurements of μ_a are optimal for τ_p that are at least one order of magnitude shorter than τ_{sr} (Fig. 5). Such conditions are readily achieved at visible and near-infrared wavelengths due to the availability of commercial Q-switched lasers emitting pulses of $\tau_p \approx 1-10$ ns. However, in the midinfrared, typical solid-state lasers emit laser pulses that are too long to satisfy the criterion $\tau \leqslant 0.1\tau_{sr}$. The Q-switched Ho:YAG and Er:YAG ($\lambda = 2.94$ μm) lasers used in this and other photoacoustics studies[11–13] emitted pulses of $\tau_p \geqslant 100$ ns. At these wavelengths, water μ_a is 28 and $\sim$10 000 cm^{-1}, respectively, corresponding to τ_{sr} of 239 and $\sim$0.7 ns, respectively. Thus, the lasers available in our laboratories were not able to emit sufficiently short laser pulses for optimal stress confinement. An alternative laser system to use is a tunable optical parametric oscillator (OPO). Unfortunately, at the time of these measurements, the OPO sys-

TABLE I. Summary of experimental and modeling data. τ_p = pulse duration, τ_{sr} = stress relaxation time, $\tau = \tau_p/\tau_{sr}$, $\mu_{a,\text{meas}}$ = measured absorption coefficient, $\mu_{a,\text{pred}}$ = model prediction of sample absorption coefficient, $\mu_{a,\text{med}}$ = literature value of water absorption coefficient.

Wavelength [μm]	τ_p [ns]	τ_{sr} [ns]	τ (-)	$\mu_{a,\text{meas}}$ [cm^{-1}]	$\mu_{a,\text{pred}}$ [cm^{-1}]	$\mu_{a,\text{med}}$ [cm^{-1}]	% improvement
2.1	815	239	3.4	21.87 ± 4.29	33.64 ± 4.33	27.92	1
2.4	4000	133	30.0	21.29 ± 1.96	64.32 ± 14.70	50.06	29
3.7	100	55	1.8	77.20 ± 3.15	100.18 ± 10.10	122.27	19
3.7	200	55	3.7	72.58 ± 2.17	147.60 ± 22.89	122.27	20
3.7	500	55	9.2	69.94 ± 1.85	159.70 ± 22.05	122.27	12
3.7	1000	55	18.3	70.81 ± 3.78	176.56 ± 30.73	122.27	−2
3.7	2000	55	36.7	70.91 ± 2.47	159.82 ± 23.42	122.27	11

tems at our institutions did not emit pulses of sufficient energy to generate measurable stress signals at midinfrared laser wavelengths. A recent study by Kostli *et al.*[14] employed an OPO for photoacoustic characterization of cartilage and chicken breast at wavelengths between 1.86 and 1.94 μm, close to the wavelengths investigated in this study. Further development of OPO technology will provide hopefully the means to characterize soft tissue μ_a at wavelengths in the 2–10 μm range without the need for deconvolution.

Two regions can be identified from the representative data set shown in Fig. 6. The first region involves a monotonic linear relationship between $\mu_{a,\mathrm{pred}}$ and $\mu_{a,\mathrm{guess}}$. The second region consists of a relatively large scatter in the data points. The values of $\mu_{a,\mathrm{pred}}$ seem to fall around a line with a positive slope, but this slope is considerably smaller than that of the first region. For smaller values of τ, the model predictions $\mu_{a,\mathrm{pred}}$ and measured values match in the first region. As τ increases, $\mu_{a,\mathrm{pred}}$ and $\mu_{a,\mathrm{meas}}$ tend to match in the second region, resulting in larger error in the estimate of $\mu_{a,\mathrm{mod}}$.

Oraevsky *et al.*[5] noted that for experimental conditions in which $\tau_p \gg \tau_{sr}$, the stress signal resembles the laser pulse temporal profile. When this limit is reached, all input values of $\mu_{a,\mathrm{guess}}$ into the deconvolution model results in similar values of $\mu_{a,\mathrm{pred}}$. The presence of the second region (Fig. 6) indicates that this limit is being approached for larger values of $\mu_{a,\mathrm{guess}}$. Thus, the model is limited in its ability to estimate $\mu_{a,\mathrm{meas}}$ for extremely large values of τ. Further studies need to be conducted to determine the value of τ over which the utility of the model is limited due to excessive stress wave propagation during the laser pulse.

Using photoacoustics, measurements of water μ_a were obtained for different τ (Table I). In general, as τ increased, the discrepancy between $\mu_{a,\mathrm{meas}}$ and $\mu_{a,\mathrm{med}}$ increased due to stress wave propagation during the laser pulse to regions outside of δ. Thus, standard photoacoustics provide limited information under conditions of $\tau_p > \tau_{sr}$. Application of a numerical deconvolution routine (Fig. 4) to the data resulted in equivalent or markedly improved knowledge of $\mu_{a,\mathrm{med}}$. With the model, the relative error was reduced by up to 30%. In this study, we allowed $\mu_{a,\mathrm{guess}}$ values with corresponding $\mu_{a,\mathrm{pred}}$ values falling within the 95% confidence interval of $\mu_{s,\mathrm{meas}}$ to be used as possible guesses for μ_a. Other approaches may improve further the accuracy of this model-based approach for correction of μ_a measurements with photoacoustics. By incorporating the acoustic transducer impulse response in the deconvolution computation,[15] further improvement is expected. Nevertheless, the improved accuracy of our approach is apparent from the results in Table I.

V. CONCLUSIONS

The purpose of this study was to investigate the effects of τ_{sr} and τ_p on μ_a values determined from photoacoustic-based measurements. For one representative set of experimental conditions, theoretical computation suggested that $\tau_p \leq 0.1\tau_{sr}$ for optimal determination of μ_a. Since it is difficult to achieve such conditions at midinfrared wavelengths due to the relatively long τ_p of commercial lasers and high μ_a of water, we developed a numerical deconvolution scheme to overcome this limitation of conventional photoacoustics. Use of the deconvolution-enhanced technique resulted in up to a 30% improvement in photoacoustic-based estimates of $\mu_{a,\mathrm{med}}$. Future studies are planned to apply this technique to measurements of stress signals from biological hard and soft tissue.

ACKNOWLEDGMENTS

The authors thank Michelle Baltz, Mike Papantonakis, Stephen Uhlhorn, Dr. Richard Haglund, and Dr. Bill Gabella for their assistance with the FEL setup; and Dr. Alexander Oraevsky and Dr. Alexander Karabutov for their instruction on TRSD measurements. Funding for this research was provided in part by grants from the Air Force Office of Scientific Research through MURI from DDR&E (F49620-98-1-0480), the Texas Higher Education Coordinating Board (BER-ATP-253), the Albert and Clemmie Caster Foundation, and the ''Medical Free Electron Laser Beam Delivery for Human Care'' part of the ''Medical & Materials Research with Free Electron Laser,'' ONR Contract No. N00014-94-1-1023.

[1] J. W. Pickering, S. A. Prahl, N. van Wieringen, J. F. Beek, H. J. C. M. Sterenborg, and M. J. C. van Gemert, Appl. Opt. **32**, 399 (1993).
[2] S. A. Prahl, M. J. C. van Gemert, and A. J. Welch, Appl. Opt. **32**, 559 (1993).
[3] T. E. Milner, D. M. Goodman, B. S. Tanenbaum, and J. S. Nelson, J. Opt. Soc. Am. A **12**, 1479 (1995).
[4] S. A. Prahl, I. A. Vitkin, U. Bruggemann, B. C. Wilson, and R. R. Anderson, Phys. Med. Biol. **37**, 1203 (1992).
[5] A. A. Oraevsky, S. L. Jacques, and F. K. Tittel, Appl. Opt. **36**, 402 (1997).
[6] J. A. Viator, S. L. Jacques, and S. A. Prahl, IEEE J. Sel. Top. Quantum Electron. **5**, 989 (1999).
[7] G. M. Hale and M. R. Querry, Appl. Opt. **12**, 555 (1973).
[8] K. Becker, J. B. Johnson, and G. Edwards, Rev. Sci. Instrum. **65**, 1496 (1994).
[9] J. M. Khosrofian and B. A. Garetz, Appl. Opt. **22**, 3406 (1983).
[10] W. H. Press, B. P. Flannery, S. A. Teukolsky, and W. T. Vetterling, *Numerical Recipes in C* (Cambridge University Press, Cambridge, 1988).
[11] K. F. Chan, B. Choi, J. M. H. Teichman, and A. J. Welch, Lasers Surg. Med. Suppl. **12**, 49 (2000).
[12] B. Choi, K. F. Chan, and A. J. Welch, Lasers Surg. Med. Suppl. **12**, 4 (2000).
[13] B. Choi, Ph.D. dissertation, The University of Texas at Austin, 2001.
[14] K. P. Kostli, M. Frenz, H. P. Weber, G. Paltauf, and H. Schmidt-Kloiber, J. Appl. Phys. **88**, 1632 (2000).
[15] G. Ku and L. V. Wang, Med. Phys. **27**, 1195 (2000).